journal

J. Am. Ceram. Soc., 82 [2] 351–58 (1999)

Effect of Bottom Electrode Materials and Annealing Treatments on the Electrical Characteristics of $Ba_{0.47}Sr_{0.53}TiO_3$ Film Capacitors

Ming-Shiahn Tsai, Shi-Chung Sun,† and Tseung-Yuen Tseng*

Department of Electronics Engineering and Institute of Electronics, National Chiao Tung University, Hsinchu 30050, Taiwan, Republic of China

The dielectric constant and leakage current density of $Ba_{0.47}Sr_{0.53}TiO_3$ (BST) thin films deposited by radio-frequency magnetron sputtering on various bottom electrode materials (Pt, Ir, IrO_2/Ir, Ru, RuO_2/Ru) before and after annealing in O_2 and N_2 ambient were investigated. Improvement in crystallinity of BST films deposited on various bottom electrodes was observed with annealing. The refractive index, dielectric constant, loss tangent, and leakage current of the films were also strongly dependent on annealing conditions. A BST thin film deposited on an Ir bottom electrode at 500°C, after 700°C annealing in O_2 for 20 min, had a dielectric constant of 593 ± 5%, a loss tangent of 0.019 ± 10% at 100 kHz, a leakage current of (2.1 ± 13%) × 10^{-8} A/cm^2 at an electric field of 100 kV/cm with a delay time of 30 s, and a charge storage density of 53 ± 5% fC/μm^2 at an applied field of 150 kV/cm. Based on the dielectric constant, leakage current, and reliability, the optimum material for the bottom electrode with annealing was Ir. Interdiffusion of Ru and Ti at the interface between the BST film and Ru electrode was observed in 500°–700°C annealed samples. The 10 year lifetime of time-dependent dielectric breakdown (TDDB) studies indicated that BST on Pt, Ir, IrO_2/Ir, Ru, and RuO_2/Ru had long lifetime over 10 years of operation at a voltage bias of 1 V.

I. Introduction

Thin films with high dielectric constant have attracted great attention in recent years for use as cell capacitors for high-density dynamic random access memories (DRAMs). These films can lower the height of the storage node and simplify the cell structure.[1–5] (Ba,Sr)TiO_3 films have been reported to be the most promising capacitor materials for gigabit DRAMs because of their high dielectric constant, low leakage current density, high dielectric breakdown strength, paraelectric perovskite phase (that does not exhibit fatigue), aging, and ease of composition control.[1–9]

The electrical characteristics of (Ba,Sr)TiO_3 thin films greatly depend on deposition conditions (sputtering power, substrate temperature, sputtering ambient, gas pressure, etc.),[6,9–11] composition of the BST thin films,[3,12] bottom electrode material (e.g., Pt, Pt/Ta, Pt/TiN/Ti, Pd/Ti, Pd, etc.),[13–15] and postannealing conditions.[10,16–18] Although there is much experimental proof that annealing conditions can significantly affect the properties of the films, systematic studies of the effect of annealing conditions on the dielectric and electrical properties of (Ba,Sr)TiO_3 thin films on various bottom electrodes are still quite limited. In the practical process of fabricating semiconductor devices, several annealing processes, such as the annealing of Al in forming gas (N_2/H_2 = 95/5) at 400°C and flow of boron phosphosilicate glass films in N_2 (at ~800°C), have been used after the deposition of (Ba,Sr)TiO_3 thin films.[19] Therefore, stability in various ambients, a good diffusion barrier, and good adhesion to the surfaces encountered in microelectronics are major requirements. In Refs. 20 and 21, we have studied the effects of bottom electrode materials (Pt, Ir, IrO_2/Ir, Ru, RuO_2/Ru) on the dielectric constant and leakage current density in $Ba_{0.47}Sr_{0.53}TiO_3$ (BST) thin films and proposed them as optimum electrode materials. The structure and the electrical and dielectric properties of the films were evaluated and discussed.

The present work attempts to more thoroughly understand the effects of annealing on the dielectric constant and leakage current density in BST thin films grown on various bottom electrodes (Pt, Ir, IrO_2/Ir, Ru, RuO_2/Ru). The structure and the electrical and dielectric properties of the films are characterized and discussed.

II. Experimental Procedures

BST thin films were deposited on metal/SiO_2/(100)Si (metal = Pt, Ir, IrO_2/Ir, Ru, and RuO_2/Ru) bottom storage node electrodes by radio-frequency (rf) magnetron sputtering. Metal layers 100 nm thick were deposited on SiO_2/Si substrate using a separate rf magnetron sputtering system. The detailed deposition conditions of the BST thin films on various bottom electrodes were described in Ref. 20.

Unless otherwise mentioned, BST films ~100 and 80 nm thick were deposited at substrate temperatures of 27° and 500°C. After deposition, the BST thin films were annealed for 20–30 min at 500°–750°C in O_2, N_2, or pure N_2O atmosphere using a quartz-glass tube furnace (FN) and rapid thermal anneal (RTA) for 1–3 min at a heating rate of 100°C/s and cooling rate of 5°C/s. Finally, the 50 nm thick top Pt electrodes with diameters of 165, 255, and 350 μm were formed by sputtering and then patterned by the shadow mask process.

Film thickness was determined by ellipsometry. The structure was characterized by X-ray diffraction (XRD; Model D5000, Siemens, Karlsruhe, Germany). The chemical composition of the films (Ba/Sr = 47/53) was close to the target composition (Ba/Sr = 50/50) within a deviation of 3% on the basis of the measured results of inductively coupled plasma atomic emission spectrometry (ICP-AES; Model SCIEX ELAN 5000, Perkin Elmer, Norwalk, CT) method. Surface roughness and morphology were examined by atomic force microscopy (AFM; Nano-Scope III, Digital Instruments, Tonawanda, NY). Depth profile analysis of deposited films was performed with secondary ion mass spectrometry (SIMS; Model IMS-4f, Cameca, Courbevoíe, France) with primary ion of Cs^+ and sputtering rate of 0.5 nm/s. The capacitance–voltage (c–v) characteristic was measured on the metal–insulator–metal (MIM) structure by measuring capacitance at 100 kHz as a function of swept positive-to-negative voltage bias. The di-

B. A. Tuttle—contributing editor

Manuscript No. 190919. Received June 17, 1997; approved May 26, 1998.
Supported by the National Science Council of R.O.C. under Project No. NSC 85-2112-M009-037.
*Member, American Ceramic Society.
†Also with Taiwan Semiconductor Manufacturing Co., Ltd., Hsinchu, Taiwan.

electric constant of the films was calculated from capacitance measured at 100 kHz without bias voltage. Dielectric and loss properties were measured as a function of frequency with an impedance gain phase analyzer (Model HP4194A, Hewlett-Packard, Palo Alto, CA). Current–voltage (*I–V*) measurements were performed by measuring the current through the sample with a semiconductor parameter analyzer (Model HP4145B, Hewlett-Packard). A Pt top electrode of the BST capacitor was connected to the voltage source, and the bottom electrode was grounded. Polarity was positive when positive voltage was applied to the top electrode. Time-dependent dielectric breakdown (TDDB) measurements were performed by measuring the current–time (*I–t*) with constant voltage through the sample with the HP4145B semiconductor parameter analyzer. Experimental data reported in this paper represent multiple measurements on ten specimens.

III. Results and Discussion

Figure 1 shows the XRD patterns of BST thin films deposited on Pt bottom electrodes at 27°C and subsequently annealed for 30 min and 1 or 3 min at 750°C in O_2 and N_2 ambient. The (110) and (200) peak intensities of the BST thin films increase with increasing annealing time in O_2 and N_2 ambient. The (110) peak intensity of the films after O_2 annealing for 30 min has 3 times the intensity of that of films annealed for 3 and 1 min. All the annealed BST films are slightly crystallized. Figure 2 illustrates XRD patterns of 80 nm thick BST thin films deposited on Pt, Ir, IrO_2/Ir, Ru, and RuO_2/Ru bottom electrode materials at 500°C. The as-deposited films on Pt, Ir, and Ru show that the BST film on Ru has the stronger (110) peak and that on Pt has the weaker (110) peak. BST films deposited on Ir and Ru show stronger (110) peaks than those on IrO_2/Ir and RuO_2/Ru, respectively. A stronger and sharper perovskite (110) peak from the film deposited on Ru compared to those from the films deposited on other bottom electrodes implies an improved crystallinity and is obtained in the film on Ru. The (101) peak of RuO_2 is observed in BST on Ru, and, therefore, a thin RuO_2 layer can be formed at the interface between BST and Ru during deposition. Figures 3(a) and (b) show XRD patterns of 80 mm thick BST thin films deposited on Pt and Ir at 500°C and subsequently furnace (FN) annealed at 500°, 600°, and 700°C in O_2 ambient for 20 min. The results of these figures indicate that the (110), (100), and (200) diffraction

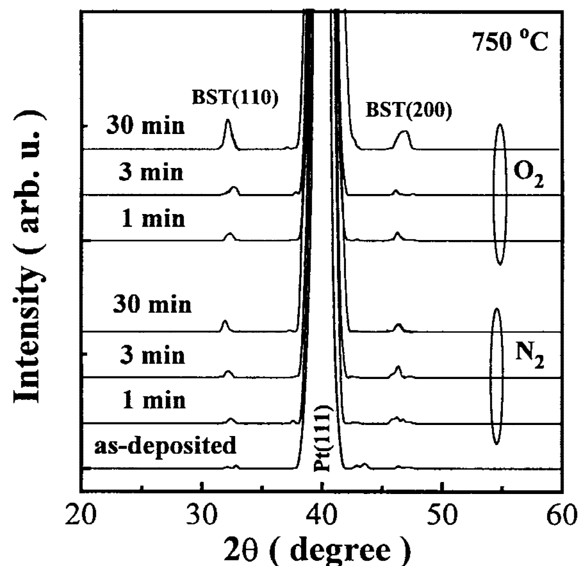

Fig. 1. XRD patterns of BST films deposited at 27°C on Pt and subsequently annealed for 30 min and 1 or 3 min at 750°C in O_2 and N_2 ambient.

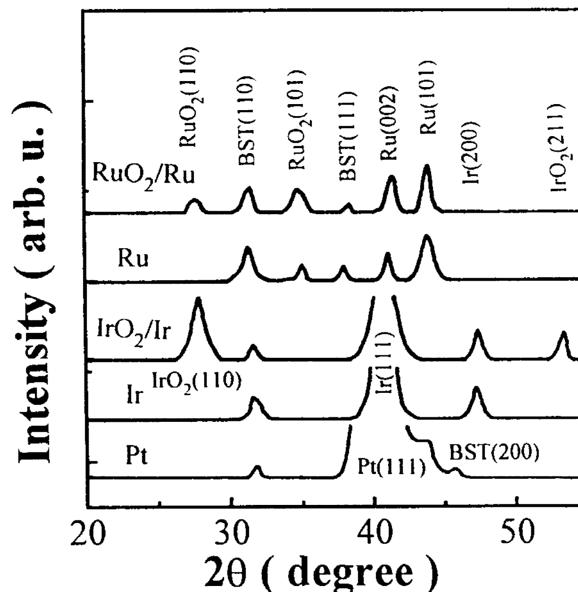

Fig. 2. XRD patterns of BST films deposited at 500°C on Pt, Ir, IrO_2/Ir, Ru, and RuO_2/Ru bottom electrodes.

peaks of BST films on Pt and Ir increase with increasing annealing temperature. Figure 3(c) shows the XRD patterns of 80 nm thick BST thin films deposited on Ru bottom electrode at 500°C and subsequently annealed under the same conditions as those in Figs. 3(a) and (b). The (111) and (100) diffraction peaks of the BST films on Ru increase with increasing annealing temperature (Fig. 3(c)). The RuO_2 (101) peaks of BST films on Ru increase as annealing temperature increases, indicating that more RuO_2 is formed at the interface between BST and Ru during annealing. XRD results suggest that improvement in the crystallinity of BST films can be achieved by annealing treatments.

Figure 4 shows that the thicknesses of BST thin films deposited on Pt at 27°C and subsequently annealed at 550°, 650°, or 750°C in N_2 ambient vary with annealing time. The thicknesses of BST films annealed at 550° and 650°C decrease with increasing annealing time. And the thickness of 750°C-annealed BST film also decreases with increasing annealing time, but it attains saturation when annealed over 1 min. XRD results suggest that, after annealing, improvement in crystallinity of the films is not observed in the 550°C-annealed film. But crystallinity of the 650°- and 750°C-annealed films is slightly improved. The thickness reductions of the films can be explained as a result of an increase in density and the elimination of porosity.

Figure 5 depicts the change in refractive index of BST thin films deposited on Pt at 27°C and subsequently annealed for 30 min and 1 or 3 min at 550°, 650°, and 750°C in N_2 ambient with annealing time. The refractive index for the BST annealed at 550°C approaches a constant value of 1.85, which is close to 1.8, the index of refraction of sputter-deposited amorphous BST.[18,22,23] The refractive indexes of the 650°- and 750°C-annealed BST increase with increasing annealing time and increase to 2.2, which approaches the refractive index (2.3) of microcrystalline BST films.[18,22,23] (The refractive index was previously shown to be affected by composition.[24]) An ICP study indicates that annealing-induced composition change in the films is not observed as long as the annealing temperature remains <750°C. Therefore, the change in the refractive index can be interpreted only as a pure annealing effect.[24] An increase in the index of refraction is usually attributed to either densification or crystallization. Densification is observed in the 550°C annealed sample (Fig. 4), but its refractive index approaches a constant value of 1.85. Slight crystallization is observed in the 650° and 750°C-annealed samples but not in the

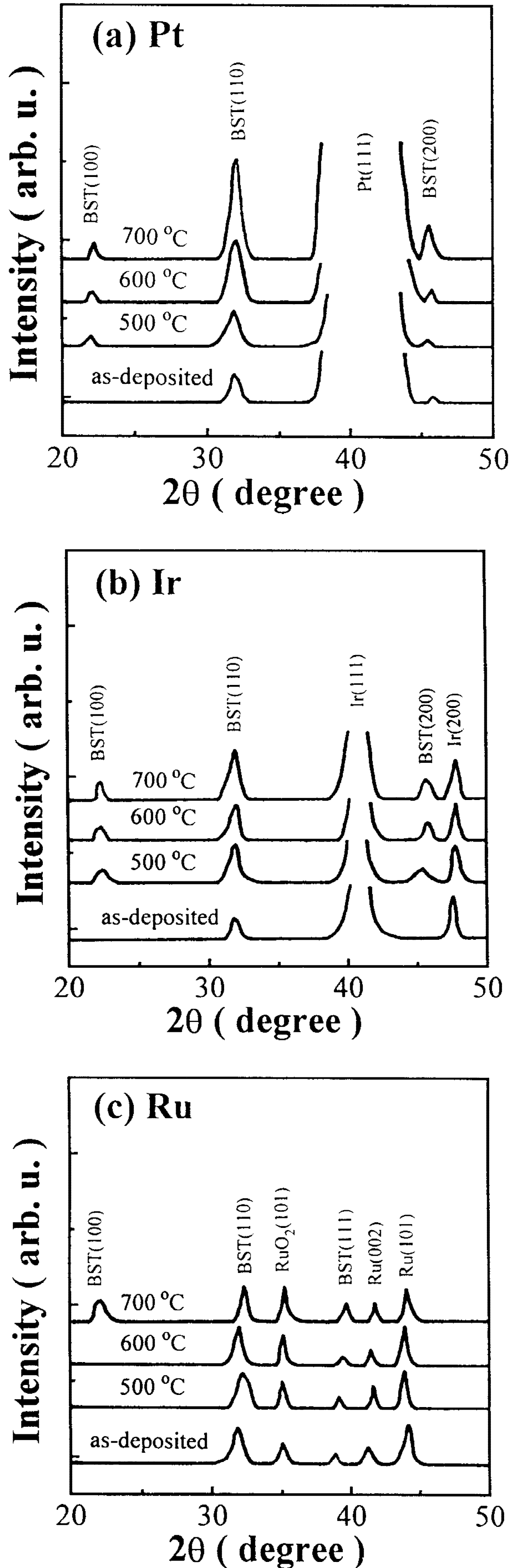

Fig. 3. XRD patterns of BST films deposited at 500°C on (a) Pt, (b) Ir, and (c) Ru and subsequently annealed for 20 min at 500°, 600°, and 700°C in O_2 ambient.

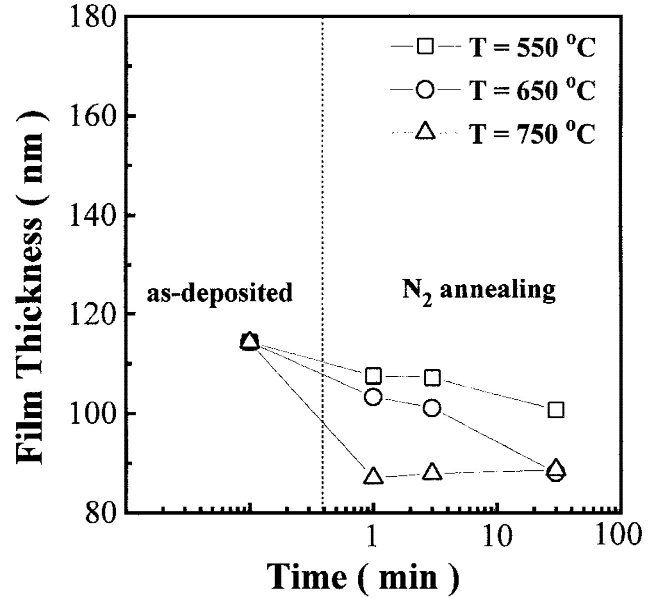

Fig. 4. Film thickness of BST films deposited at 27°C on Pt and subsequently annealed for 30 min and 1 or 3 min at 550°, 650°, and 750°C in N_2 ambient.

550°C annealed sample, based on XRD results (not shown here). In fact, both 650° and 750°C annealed samples can achieve the same refractive index of 2.2 after 30 min annealing. Therefore, the change in the index of refraction is believed to correlate with the increased crystallization of the films.

Figure 6 shows that the dielectric constant of BST thin films annealed at different temperatures varies with annealing time. The dielectric constant of BST annealed at 550°C in N_2 or O_2 ambient does not change with annealing time and approaches a constant value ~23, because its crystallinity is not improved by annealing (on the basis of XRD results). The dielectric constants of BST annealed at 650° and 750°C increase with increasing annealing time, which is attributed to the increasing crystallization of the films. The dielectric constant and refractive index of BST films vary with annealing temperature and behave similarly, as indicated in Figs. 5 and 6.

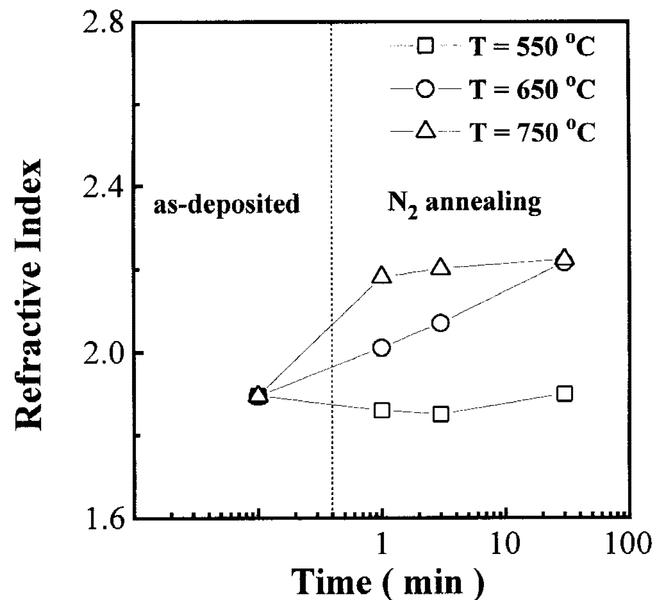

Fig. 5. Refractive index of BST films deposited at 27°C on Pt and subsequently annealed for 30 min and 1 or 3 min at 550°, 650°, and 750°C in N_2 ambient.

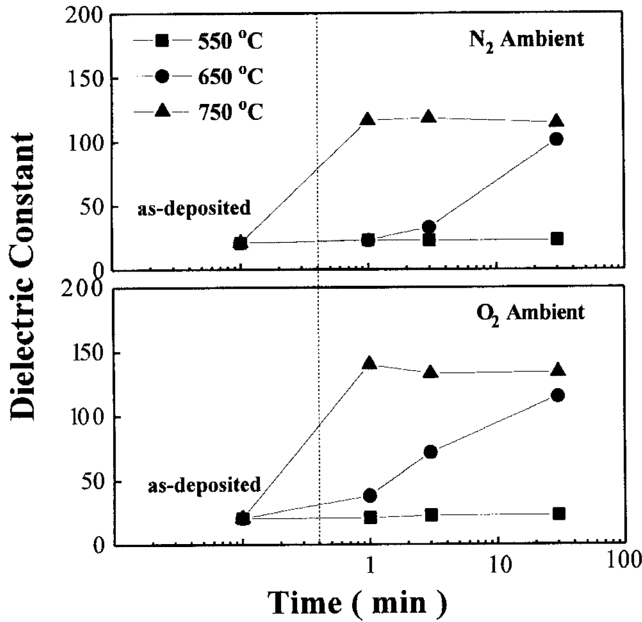

Fig. 6. Dielectric constant of BST films deposited at 27°C on Pt and subsequently annealed for 30 min and 1 or 3 min at 550°, 650°, and 750°C in N_2 and O_2 ambient.

Figure 7 shows that leakage current at 100 kV/cm with a delay time of 30 s (a transient leakage current) for BST thin films, which are deposited and annealed under the same conditions as those in Fig. 6 before top-electrode deposition, is dependent on annealing time and temperature. The leakage current of BST annealed at 550°C decreases with increasing annealing time because of increasing densification of BST films after annealing, as shown in Fig. 4. The leakage current of BST annealed at 750°C increases with increasing annealing time, because the increase in the dielectric constant of 750°C annealed film (Fig. 6) can be due to the enhanced ionic polarization and improved crystallinity with larger grain size. However, this enhanced ionic polarization increases the energy dissipation during relaxation,[24] and films with large grain size have short diffusion paths along the grain boundary, which are expected to cause an increase in the leakage current. The leakage current of BST annealed in N_2 and O_2 at 650°C decreases with increasing annealing time but slightly increases for BST films after annealing for 30 and 3 min. The possible reason is that the increasing densification of BST film after annealing (Fig. 4) leads to a decrease in the leakage current, but the resulting ionic polarization enhancement and improved crystallinity increase the leakage current. Results of the dielectric constant measurement of BST annealed in O_2 are in good agreement with the results of BST annealed in N_2, as shown in Fig. 6. On the other hand, results of the leakage current of BST annealed in O_2 are in good agreement with the results of BST annealed in N_2, as shown in Fig. 7. The dielectric constants of BST annealed in O_2 are larger than those of the BST annealed in N_2, and the leakage current of BST annealed in O_2 is smaller than the leakage current of BST annealed in N_2. The reason could be the decrease of oxygen vacancies of BST after annealing in O_2 and, hence, the dielectric constant can be enhanced and the leakage current can be decreased.

To further reduce oxygen vacancies in BST, annealing of the BST film in pure N_2O ambient was conducted, because the oxidation effect of N_2O was stronger than that of O_2. BST films deposited on Pt bottom electrodes at 27°C and annealed in N_2O ambient showed a very large leakage current, and, therefore, their dielectric properties could not be measured. The decrease of oxygen vacancies was expected in N_2O-annealed BST films. Therefore, the large leakage current observed in these films could not be attributed to oxygen vacancies and the compensating electrons. However, the ionic polarization might be enhanced in the films, which would lead to an increase in the energy dissipation during relaxation.[24] Therefore, the dielectric loss of BST films could be increased by N_2O treatments. In Ref. 25, we also observed a similar phenomenon in which the dielectric loss of BST decreased with increased oxygen deposition pressure but had a minimum value at 40% $O_2/(Ar + O_2)$. Further increase of the oxygen pressure of deposition increased the dielectric loss of the BST films. From the above data, we could predict that annealing BST films in O_2 at 600°C for 20 min was the most suitable condition for obtaining high dielectric constant and low leakage current.

The dependences of the dielectric constant and leakage current density measured at 100 kV/cm with a delay time of 30 s on the various bottom electrodes are shown in Fig. 8. This figure indicates that BST film deposited on Ru bottom elec-

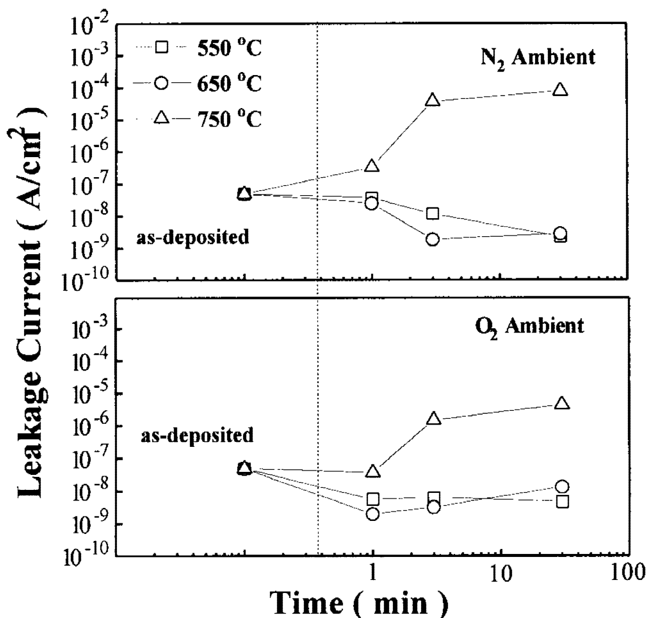

Fig. 7. Leakage current of BST films deposited at 27°C on Pt and subsequently annealed for 30 min and 1 or 3 min at 550°, 650°, and 750°C in N_2 and O_2 ambient.

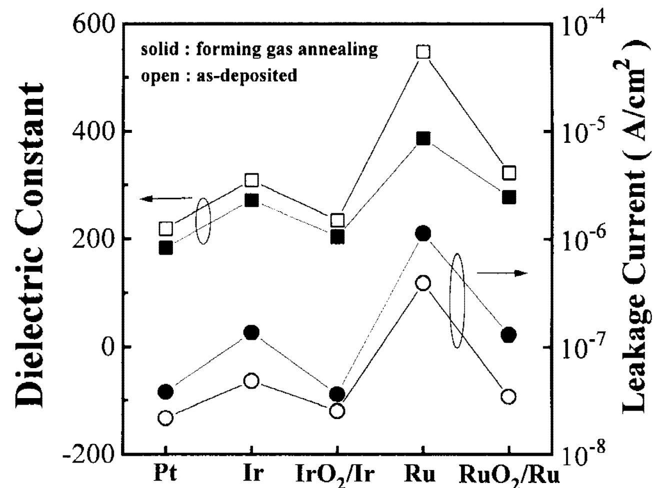

Fig. 8. Dielectric constant and leakage current of BST thin films deposited on Pt, Ir, IrO_2/Ir, Ru, and RuO_2/Ru bottom electrodes and annealed in forming gas at 400°C for 30 min.

trode has a maximum dielectric constant of 548 ± 4% and leakage current density of (3.94 ± 8%) × 10^{-7} A/cm^2. BST film deposited on Pt has a minimum dielectric constant of 219 ± 4% and a leakage current density of (2.2 ± 13%) × 10^{-8} A/cm^2. The details are described in earlier reports.[20,21] The dependences of the dielectric constant and leakage current density of BST on various bottom electrodes annealed in forming gas (N_2/H_2 = 95/5) at 400°C for 30 min before top-electrode deposition are also shown in Fig. 8. This figure indicates that BST films after annealing have lower dielectric constants and higher leakage currents, which can be attributed to induced damage during hydrogen annealing. That is, the active reduction and diffusion of hydrogen, even at temperature as low as 350°C, can cause the activated hydrogen to penetrate into the BST and bottom electrode Pt; consequently, it can lead to chemical reaction and change in the BST/Pt interface.[26–29] The damage can also take the form of oxygen vacancies, which produce positively charged centers in the BST films.

Figure 9(a) shows the variation of the dielectric constant of BST thin films, deposited on Pt, Ir, and IrO_2/Ir bottom electrode materials at 500°C and sequentially annealed in O_2 at 500°, 600°, and 700°C for 20 min. The dielectric constant increases with increasing annealing temperature, and the intensities of the XRD peaks of BST on Pt and Ir also increase with increasing annealing temperature, as shown in Figs. 3(a) and (b). Figure 9(b) shows the dielectric constant of BST thin films, deposited on Ru and RuO_2/Ru bottom electrode materials at 500°C and subsequently annealed for 20 min at 500°, 600°, and 700°C in O_2 ambient, is dependent on annealing temperature. The dielectric constant of BST on RuO_2/Ru increases with increasing annealing temperature, and the dielectric constant of BST on Ru decreases with increasing annealing temperature. Hence, BST deposited on Pt, Ir, IrO_2/Ir, and RuO_2/Ru after postannealing are more stable than BST on Ru. On the other hand, BST films deposited at 500°C with postannealing (Fig. 9) are more suitable than those deposited at 27°C with postannealing (Fig. 6) for obtaining good-quality BST films with high dielectric constants. This is because the crystallinity of BST deposited at 27°C with postannealing is inferior to that of BST deposited at 500°C with and without postannealing.

From SIMS data, we observe that the oxygen concentrations

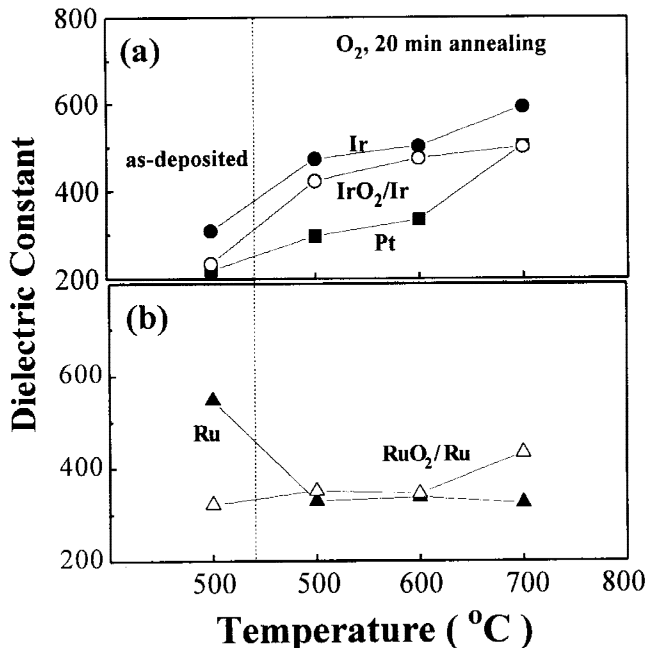

Fig. 9. Dielectric constant of BST films deposited at 500°C on (a) Pt, Ir, and IrO_2/Ir, (b) Ru and RuO_2/Ru and subsequently annealed for 20 min at 500°, 600°, and 700°C in O_2 ambient.

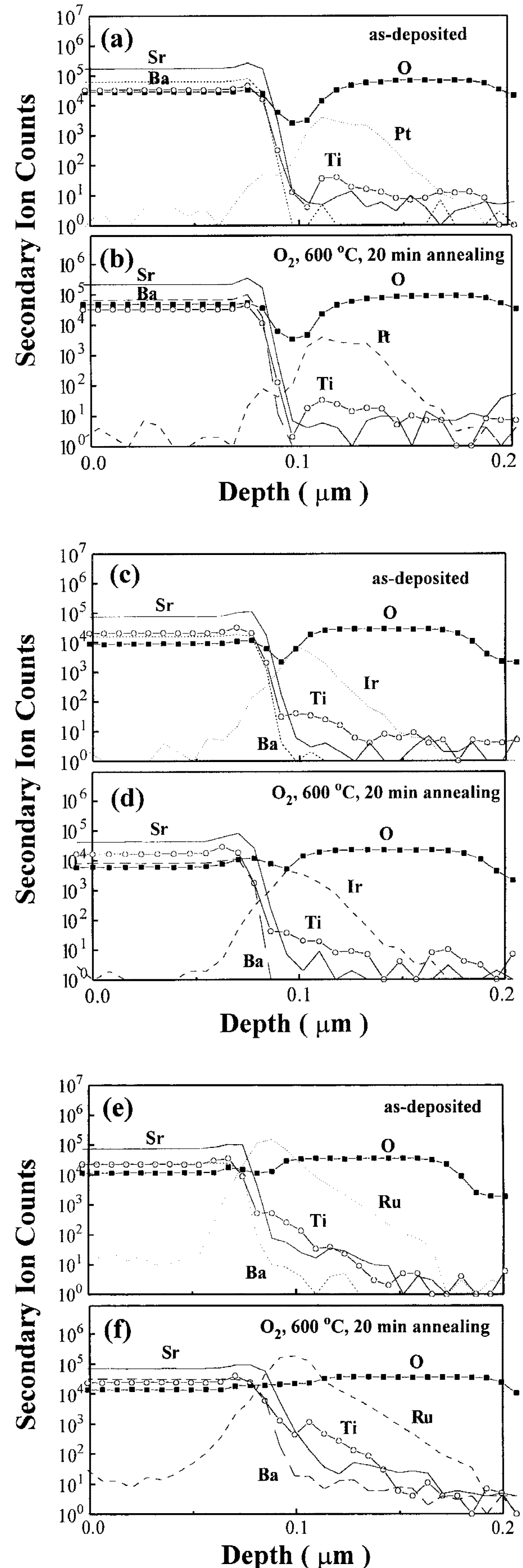

Fig. 10. SIMS profile of BST deposited on (a) Pt; (b) Pt after 600°C, O_2 annealing; (c) Ir; (d) Ir after 600°C, O_2 annealing; (e) Ru; and (f) Ru after 600°C, O_2 annealing.

at BST/Ru and BST/Ir interfaces are larger than at the BST/Pt interface, as shown in Figs. 10(a), (c), and (e). Hence, the interfaces of BST/Ru and BST/Ir can suppress the accumulation of oxygen vacancies. Figures 10(b), (d), and (f) show the SIMS data of BST deposited on Pt, Ir, and Ru and subsequently annealed in O_2 at 600°C for 20 min. Figures 10(a) and (b) of the Ti and Pt profiles of BST on Pt indicate no interdiffusion and no change in the oxygen concentration at the interface. Figures 10(c) and (d) of the Ti and Ir profiles of BST on Ir show no interdiffusion and a slight increase in the oxygen concentration at the interface. Therefore, BST films on Pt and Ir after annealing are more stable, and their dielectric constant increases with increasing annealing temperature. Figures 10(e) and (f) of the Ti and Ru profiles of BST on Ru indicate interdiffusion and a slight increase in the oxygen concentration at the interface. SIMS depth profile of the interface of BST/Ru is measured and indicated in Figs. 10(e) and (f). A thinner interfacial layer of RuO_x is formed. (Figure 3(c) shows the $RuO_2(101)$ peak before and after annealing, and Figs. 10(e) and (f) show a slight increase in the oxygen concentration at the interface.) Consequently, the leakage current of BST on Ru after annealing can approach the leakage current of BST on RuO_2/Ru (Figs. 8 and 11). The large decrease of the dielectric constant is attributed to the low dielectric interfacial layer formed between the BST and Ru because of annealing at 500°, 600°, and 700°C, as shown in Fig. 9. It is also possible that a thin interfacial layer, such as $(Ba,Sr)(Ru,Ti)O_3$, might be formed by the interdiffusion of these ions, when allowed by the thermal activation energy, because of the similarity of the ionic radii of Ru^{4+} and Ti^{4+}, as shown in Figs. 10(e) and (f). BST on IrO_2/Ir and RuO_2/Ru after annealing are more stable, similar to BST on Pt and Ir.

Figure 11 shows that the leakage current at 100 kV/cm with a delay time of 30 s for BST thin films, deposited on Pt, Ir, and Ru bottom electrodes at 500°C and subsequently annealed before top-electrode deposition under the same conditions as those in Fig. 3, is dependent on annealing temperature. There is no change in the leakage current of BST on Pt after annealing. The leakage current of BST on Ir and Ru after annealing decreases with annealing temperature. SIMS analysis (Figs. 10(c), (d), (e), and (f) shows that the interfaces of BST/Ir and BST/Ru can form a thinner interfacial layer of IrO_x and RuO_x, and, hence, the leakage current approaches the leakage current

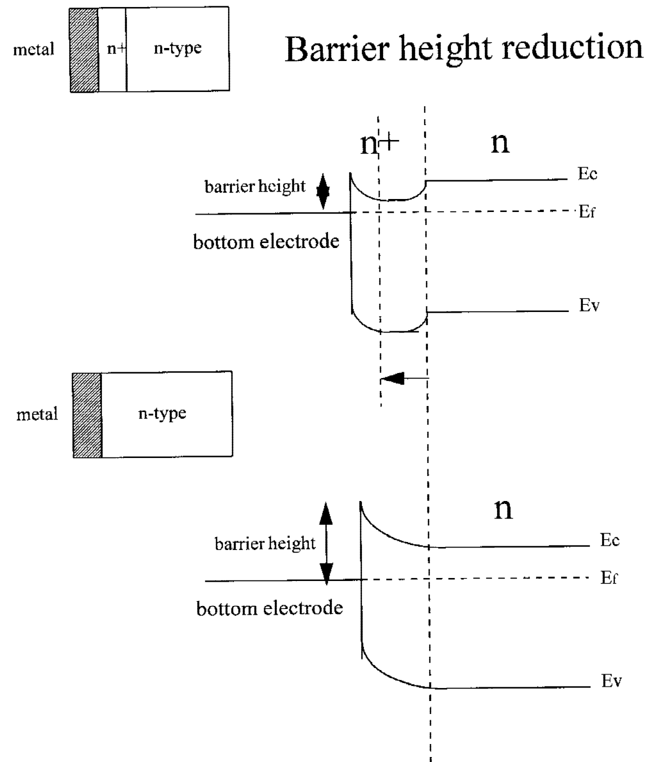

Fig. 12. Barrier height of metal–n^+-type–n-type and metal–n-type structures.

of BST on IrO_2/Ir and RuO_2/Ru (Figs. 8 and 11). The thinner interfacial layer of IrO_x and RuO_x can suppress the accumulation of oxygen vacancies at the BST/Ru and BST/Ir interfaces, and, therefore, the interfaces of BST/Ru and BST/Ir before annealing have a greater accumulation of oxygen vacancies than the interfaces of BST/Ru and BST/Ir after annealing. The oxygen vacancy acts as a donor dopant, and, hence, the BST material tends to show n-type conductivity. The number of oxygen vacancies accumulated at the interface is larger, and the interface tends to show n^+-type conductivity. Hence, BST/Ru

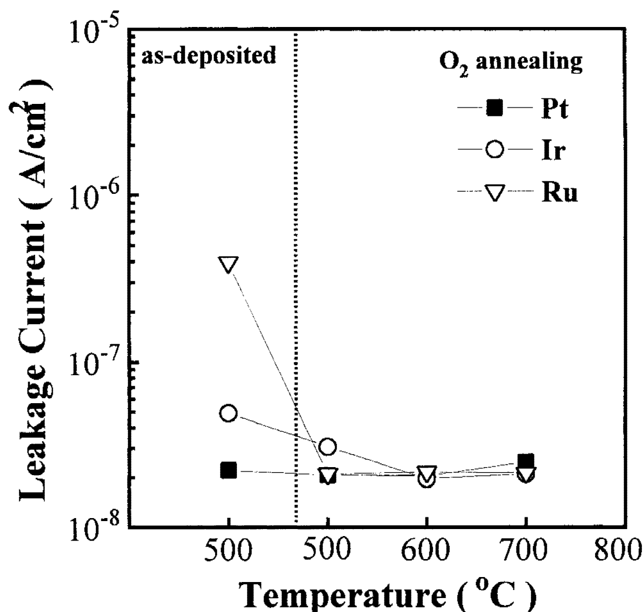

Fig. 11. Leakage current of BST films deposited at 500°C on Pt, Ir, and Ru and subsequently annealed for 20 min at 500°, 600°, and 700°C in O_2 ambient.

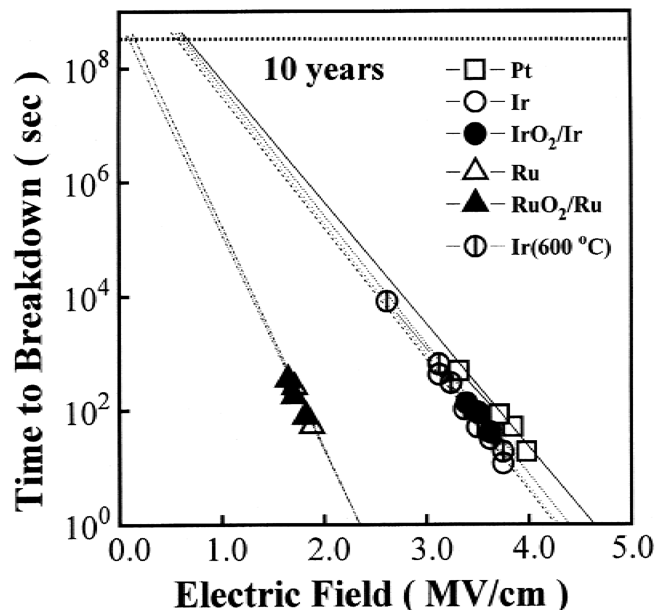

Fig. 13. Time-to-breakdown of the BST films on various bottom electrodes as a function of electric field.

Table I. Properties of BST Thin Films Deposited on Various Bottom Electrode Materials

Property	Bottom Electrode				
	Pt	Ir	IrO_2/Ir	Ru	RuO_2/Ru
Dielectric constant†	219 ± 4% (503 ± 5%)	309 ± 3% (593 ± 5%)	234 ± 4% (501 ± 6%)	548 ± 4% (325 ± 4%)	322 ± 3% (433 ± 4%)
Leakage current at 100 kV/cm (10^{-8}A/cm^2)†	2.2 ± 13% (2.5 ± 12%)	4.9 ± 12% (2.1 ± 13%)	2.5 ± 12% (3.3 ± 10%)	39.4 ± 8% (2.1 ± 12%)	3.5 ± 11% (2.4 ± 13%)
Loss tangent†	0.014 ± 9% (0.015 ± 9%)	0.046 ± 6% (0.019 ± 10%)	0.016 ± 9% (0.02 ± 10%)	0.32 ± 6% (0.019 ± 10%)	0.017 ± 9% (0.012 ± 11%)
Work function (eV)	5.6	5.35		4.8	
Fatigue endurance (cycling number)	$>10^{11}$	$>10^{11}$	$>10^{11}$	$>10^{11}$	$>10^{11}$
BST surface roughness (nm)	1.9	1.27	2.25	4.40	4.12
H_2 damage endurance (dielectric constant variation) (%)	−16	−12	−13	−29	−14
Stability in O_2 ambient (°C)	≤700	≤700	≤700	≤500	≤700

†Numbers in parentheses are after annealing for 20 min at 700°C in O_2.

and BST/Ir structures before annealing are similar to the n-type–n^+-type–metal structure, and BST/Ru and BST/Ir structures after annealing are similar to the n-type–metal structure. Based on the physics of semiconductor devices, the n-type–n^+-type–metal structure results in barrier height reduction, so that the n-type–metal structure has larger barrier height than the n-type–n^+-type–metal structure, as shown in Fig. 12. Therefore, the leakage current of BST on Ir and Ru after annealing decreases with annealing temperature, because the barrier height of BST on Ir and Ru after annealing increases with annealing temperature.

Lifetime extrapolation using constant-voltage–stress time-dependent dielectric breakdown studies (Fig. 13) predicts 10 year lifetime at 1 V operating voltage. The studies indicate that BST on Pt, Ir, Ir (600°C) (BST annealed in O_2 at 600°C for 20 min), and IrO_2/Ir samples have a longer lifetime at 1 V operating voltage than BST on Ru and RuO_2/Ru. TDDB is also referred to as resistance degradation of dielectrics, which shows a slow increase of leakage current under dc field stress. TDDB is characteristic of the intrinsic materials, the procedures and quality of the processing, and electrode materials.[30,31] The 10 year lifetime of TDDB studies indicates that BST on Pt, Ir, IrO_2/Ir, Ru, and RuO_2/Ru has a lifetime over 10 years of operation at a voltage bias of 1 V. There are several models describing the phenomena of TDDB.[32–37] The details are described in earlier reports.[32,33] The effects of bottom electrodes on the properties of BST film capacitors are summarized in Table I.

IV. Conclusions

The crystallinity and electrical properties of BST films deposited on Pt, Ir, IrO_2/Ir, Ru, and RuO_2/Ru bottom electrodes strongly depend on annealing conditions. We have shown that a BST thin film deposited on Ru at 500°C has a dielectric constant of 548 ± 4%, a loss tangent of 0.32 ± 6% at 100 kHz, a leakage current of (3.94 ± 8%) × 10^{-7} A/cm^2 at an electric field of 100 kV/cm with a delay time 30 s, and a charge storage density of 49 ± 4% fC/μm^2 at an applied field of 150 kV/cm. After the BST deposited on Ru capacitor is annealed in O_2 at 700°C for 20 min, the loss tangent decreases to 0.019 ± 10% and the leakage current decreases to (2.1 ± 12%) × 10^{-8} A/cm^2 at an electric field of 100 kV/cm with a delay time of 30 s. A BST thin film deposited on Ir at 500°C after 700°C annealing in O_2 for 20 min has a dielectric constant of 593 ± 5%, a loss tangent of 0.019 ± 10% at 100 kHz, a leakage current of (2.1 ± 13%) × 10^{-8} A/cm^2 at an electric field of 100 kV/cm with a delay time 30 s, and a charge storage density of 53 ± 5% fC/μm^2 at an applied field of 150 kV/cm. Based on the dielectric constant, leakage current, and reliability, the optimum material for the bottom electrode with annealing is Ir. The Ru electrode is unstable, because interdiffusion of Ru and Ti occurs at the interface between BST and Ru after annealing. The extrapolated 10 year lifetime of TDDB studies indicates that BST films on Pt, Ir IrO_2/Ir, and Ir (600°C) have a longer lifetime at 1 V operating voltage than those on Ru and RuO_2/Ru.

Acknowledgment: Dr. P. Lin is thanked for helpful discussions.

References

[1]Y. Ohno, T. Horikawa, H. Shinkawata, K. Kashihara, T. Kuroiwa, T. Okudaira, Y. Hashizume, K. Fukumoto, T. Eimori, T. Shibano, K. Arimoto, H. Itoh, T. Nishimura, and H. Miyoshi, ''A Memory Cell Capacitor with $Ba_xSr_{1-x}TiO_3$ (BST) Film for Advanced DRAMs,'' *Symp. VLSI Tech. Dig. Tech. Pap.*, 149–50 (1994).

[2]T. Eimori, Y. Ohno, J. Matsufusa, S. Kishimura, A. Yoshida, H. Sumitani, T. Maruyama, Y. Hayashide, K. Moriizumi, T. Katayama, M. Asakura, T. Horikawa, T. Shibano, H. Itoh, K. Namba, T. Nishimura, S. Satoh, and H. Miyoshi, ''A Newly Designed Planar Stacked Capacitor Cell with High Dielectric Constant Film for 256 Mbit DRAM,'' *IEDM Tech. Dig.*, 631–34 (1993).

[3]E. Fujii, Y. Uemoto, S. Hayashi, T. Nasu, Y. Shimada, A. Matsuda, M. Kibe, M. Azuma, T. Otsuki, G. Kano, M. Scott, L. D. Mcmillan, and C. A. Paz de Araujo, ''ULSI DRAM Technology with $Ba_{0.7}Sr_{0.3}TiO_3$ Film of 1.3 nm Equivalent SiO_2 Thickness and 10^{-9} (A/cm^2) Leakage Current,'' *IEDM Tech. Dig.*, 267–70 (1992).

[4]K. Koyama, T. Sakuma, S. Yamamichi, H. Watanabe, H. Aoki, S. Ohya, Y. Miyasaka, and T. Kikkawa, ''A Stacked Capacitor with $Ba_xSr_{1-x}TiO_3$ for 256M DRAM,'' *IEDM Tech. Dig.*, 823–26 (1991).

[5]T. Y. Tseng, ''Fabrication and Characterization of Electroceramic Thin Films for Semiconductor Memory Applications,'' *Proc. Int. Electron Devices Mater. Symp.*, **C2–5**, 89–96 (1996).

[6]T. Horikawa, N. Mikami, T. Makita, J. Tanimura, M. Kataoka, K. Sato, and M. Nunoshita, ''Dielectric Properties of (Ba,Sr)TiO_3 Thin Film Deposited by rf Sputtering,'' *Jpn. J. Appl. Phys.*, **32**, 4216–30 (1993).

[7]T. Kuoiwa, Y. Tsunenine, T. Horikawa, T. Makita, J. Tanimura, N. Mikami, and K. Sato, ''Dielectric Properties of $(Ba_xSr_{1-x})TiO_3$ Thin Films Prepared by rf Sputtering for Dynamic Random Access Memory Application,'' *Jpn. J. Appl. Phys.*, **33**, 5187–91 (1994).

[8]R. Khamankar, B. Jiang, R. Tsu, W. Y. Hsu, J. Nulman, S. Summerfelt, M. Anthony, and J. Lee, ''A Novel Low-Temperature Process for High Dielectric Constant BST Thin Films for ULSI DRAM Applications,'' *Symp. VLSI Tech. Dig. Tech. Pap.*, 127–28 (1995).

[9]S. G. Yoon and A. Safari, ''$(Ba_{0.5},Sr_{0.5})TiO_3$ Thin Film Preparation by rf Magnetron Sputtering and Its Electric Properties,'' *Thin Solid Films*, **254**, 211–15 (1995).

[10]S. O. Park, C. S. Hwang, H. J. Cho, C. S. Kang, H. K. Kang, S. I. Lee, and M. Y. Lee, ''Fabrication and Electrical Characterization of Pt/(Ba,Sr)TiO_3/Pt Capacitors for Ultralarge-Scale Integrated DRAM Applications,'' *Jpn. J. Appl. Phys.*, **35**, 1548–52 (1996).

[11]S. C. Sun, M. S. Tasi, P. Lin, J. A. Lay, D. C. H. Yu, and M. S. Liang, ''Effect of Oxygen to Argon Ratio on Properties of (Ba,Sr)TiO_3 Thin Films Prepared by rf Sputtering,'' *ECS Meet. Abstr.*, **96–1**, 184–85 (1996).

[12]H. Kobayashi and T. Kobayashi, ''Heteroepitaxial Growth of Quaternary $Ba_xSr_{1-x}TiO_3$ Thin Films by ArF Excimer Laser Ablation,'' *Jpn. J. Appl. Phys.*, **33**, L533–L536 (1994).

[13]W. J. Lee, I. K. Park, G. E. Jang, and H. G. Kim, ''Electrical Properties and Crystal Structure of $(Ba_{0.5},Sr_{0.5})TiO_3$ Thin Films Prepared on Pt/SiO_2/Si by rf Magnetron Sputtering,'' *Jpn. J. Appl. Phys.*, **34**, 196–99 (1995).

[14]K. Takemura, S. Yamamichi, P. Y. Lesaicherre, K. Tokashiki, H. Miyamoto, H. Ono, Y. Miyasaka, and M. Yoshida, ''RuO_2/TiN-Based Storage Electrodes for (Ba,Sr)TiO_3 Dynamic Random Access Memory Capacitors,'' *Jpn. J. Appl. Phys.*, **34**, 5224–29 (1995).

[15]T. Sakuma, S. Yamamichi, S. Matsubara, H. Yamaguchi, and Y. Miyasaka, ''Barrier Layers for Realization of High Capacitance Density in $SrTiO_3$ Thin Film Capacitor on Silicon,'' *Appl. Phys. Lett.*, **57**, 2431–33 (1990).

[16]Y. Fukuda, K. Numata, K. Aoki, and A. Nishimura, ''Origin of Dielectric Relaxation Observed for $Ba_{0.5}Sr_{0.5}TiO_3$ Thin Film Capacitor,'' *Jpn. J. Appl. Phys.*, **35**, 5178–80 (1996).

[17]C. S. Hwang, S. O. Park, H. J. Cho, C. S. Kang, H. K. Kang, S. I. Lee, and M. Y. Lee, ''Deposition of Extremely Thin (Ba,Sr)TiO_3 Thin Films for Ultra Large Scale Integrated Dynamic Random Access Memory Application,'' *Appl. Phys. Lett.*, **67**, 2819–21 (1995).

[18]N. Ichinose and T. Ogiwara, ''Preparation and Rapid Thermal Annealing Effect of (Ba,Sr)TiO_3 Thin Films,'' *Jpn. J. Appl. Phys.*, **34**, 5198–201 (1995).

[19]H. Matsuhashi and S. Nishikawa, ''Optimum Electrode Materials for Ta_2O_5 Capacitors for High and Low Temperature Processes,'' *Jpn. J. Appl. Phys.*, **33**, L293–L297 (1994).

[20]M. S. Tsai, S. C. Sun, and T. Y. Tseng, ''Effect of Bottom Electrode Materials on the Electrical and Reliability Characteristics of (Ba,Sr)TiO_3 Capacitors,'' *IEEE Trans. Electron Devices*, in review.

[21]S. C. Sun and M. S. Tsai, ''Effect of Bottom Electrode Materials on the Electrical and Reliability Characteristics of (Ba,Sr)TiO_3 Capacitors,'' *IEDM Tech. Dig.*, Session 10.3 (1997).

[22]M. Yoshida, H. Yamaguchi, T. Sakuma, and Y. Miyasaka, ''Chemical Vapor Deposition of (Ba,Sr)TiO_3,'' *J. Electrochem. Soc.*, **142**, 244–48 (1995).

[23]T. S. Kim, M. H. Oh, and C. H. Kim, ''Influences of Indium Tin Oxide Layer on the Properties of rf Magnetron-Sputtered (Ba,Sr)TiO_3 Thin Films on Indium Tin Oxide-Coated Glass Substrate,'' *Jpn. J. Appl. Phys.*, **32**, 2837–41 (1993).

[24]P. Li, J. F. Mcdonald, and T. M. Lu, ''Densification Induced Dielectric Properties Change in Amorphous $BaTiO_3$ Thin Films,'' *J. Appl. Phys.*, **71**, 5596–600 (1992).

[25]M. S. Tsai, S. C. Sun, and T. Y. Tseng, ''Effect of Oxygen to Argon Ratio on Properties of (Ba,Sr)TiO_3 Thin Films Prepared by Radio-Frequency Magnetron Sputtering,'' *J. Appl. Phys.*, **82** [7] 3482–87 (1997).

[26]R. Khamankar, J. Kim, B. Jiang, C. Sudhama, P. Maniar, R. Moazzami, R. Jones, and J. Lee, ''Impact of Post Processing Damages on the Performance of High Dielectric Constant PLZT Thin Film Capacitors for ULSI DRAM Application,'' *VLSI Tech. Dig.*, 119–21 (1995).

[27]H. Miki, K. K. Abdelghafar, K. Torii, and Y. Fujisaki, ''Hydrogen-Related Degradation and Recovery Phenomena in Pb(Zr,Ti)O_3 Capacitors with a Platinum Electrode,'' *Jpn. J. Appl. Phys.*, **36**, 1132–35 (1997).

[28]S. Takatani, K. K. Abdelghafar, and H. Miki, ''Effect of H_2 Annealing on a Pt/$PbZr_xTi_{1-x}O_3$ Interface Studied by X-ray Photoelectron Spectroscopy,'' *Jpn. J. Appl. Phys.*, **36**, L435–L438 (1997).

[29]Y. Shimamoto, K. K. Abdelghafar, H. Miki, and Y. Fujisaki, ''H_2 Damage of Ferroelectric Pb(Zr,Ti)O_3 Thin Film Capacitors—The Role of Catalytic and Adsorptive Activity of the Top Electrode,'' *Appl. Phys. Lett.*, **70**, 3096–97 (1997).

[30]L. H. Parker and A. F. Tasch, ''Ferroelectric Material for 64 Mb DRAMs,'' *IEEE Circuits Devices Mag.*, 17–26 (1990).

[31]P. Hiergeist, A. Spitzer, and S. Rohl, ''Lifetime of Thin Oxide and Oxide–Nitride–Oxide Dielectrics within Trench Capacitors for DRAM's,'' *IEEE Trans. Electron Devices*, **36**, 913–19 (1989).

[32]M. S. Tsai and T. Y. Tseng, ''Conduction Mechanisms and Temperature-Dependent Current–Voltage in (Ba,Sr)TiO_3 Thin Films,'' *J. Electrochem. Soc.*, **145** [8] 2853–60 (1998).

[33]M. S. Tsai and T. Y. Tseng, ''Effect of Bottom Electrodes on Resistance Degradation and Breakdown of (Ba,Sr)TiO_3 Thin Films,'' *IEEE Trans. Compon. Packag. Manuf. Technol.—A*, submitted.

[34]G. W. Dietz, W. Antpohler, M. Klee, and R. Waser, ''Electrode Influence on the Charge Transport through $SrTiO_3$ Thin Films,'' *J. Appl. Phys.*, **78**, 6113–21 (1995).

[35]G. W. Dietz, M. Schumacher, R. Waser, S. K. Streiffer, C. Basceri, and A. I. Kingon, ''Leakage Current in $Ba_{0.7}Sr_{0.3}TiO_3$ Thin Films for Ultrahigh Density Dynamic Random Memories,'' *J. Appl. Phys.*, **82**, 2359–64 (1997).

[36]R. Waser, T. Baiatu, and K. H. Hardtl, ''DC Electrical Degradation of Perovskite Type Titanates: I, Ceramics,'' *J. Am. Ceram. Soc.*, **73**, 1645–53 (1990).

[37]R. M. Waser, ''Electrochemical Boundary Conditions for Resistance Degradation of Doped Alkaline-Earth Titanates,'' *J. Am. Ceram. Soc.*, **72**, 2234–40 (1989). □